Utilizing 3D-DIC on the Mars 2020 Rover Wheel Assembly: Test-Analysis Correlation

Nathaniel W. Gardner
NASA Langley Research Center
Hampton, VA 23681
Nathaniel.W.Gardner@nasa.gov

Sotiris Kellas
NASA Langley Research Center
Hampton, VA 23681
Sotiris.Kellas@nasa.gov

Jonathan C. Hamel
NASA Jet Propulsion Laboratory
California Institute of Technology
Pasadena, CA 91109
Jonathan.C.Hamel@jpl.nasa.gov

Abstract— **Following the successful implementation of full-field photogrammetry, more specifically three-dimensional digital image correlation (3D-DIC), on the Mars 2020 Heat Shield Structural Failure Review assessment, 3D-DIC was selected as one of the primary measurement techniques for the Mars 2020 Rover wheel assembly qualification test at the NASA Jet Propulsion Laboratory (JPL). To validate the Rover wheel landing loads simulations, it was extremely important to have high confidence in the wheel models. Due to the large deformations and strains that the wheel would be subject to during landing, traditional instrumentation such as linear variable displacement transducers (LVDTs), electrical-resistance strain gages and string potentiometers, would not be sufficient on their own to provide all the necessary validation data. Therefore, the NASA Engineering and Safety Center (NESC) provided the 3D-DIC expertise and support to measure the high deformation and strain in the wheel flexures and qualify the overall structural response of the Mars 2020 rover wheel assembly. There were two key objectives for the photogrammetry technique: (1) monitor the wheel response in real-time, guarding against anomalous behavior and failure, and (2) provide test data for test-analysis correlation to validate and/or improve the high-fidelity computational model. The contents of this paper will focus on the challenges of applying 3D-DIC to the Mars 2020 Rover wheel assembly and how these challenges were overcome. Examples of test-analysis correlation during the stiffness characterization and structural qualification will be presented and discussed in detail. Experimental results were compared with the analysis and showed excellent agreement between the predicted behavior and helped validate the high-fidelity models.**

TABLE OF CONTENTS

1. INTRODUCTION

In August of 2012, the Mars Science Laboratory (MSL) Curiosity Rover landed on Mars and began the surface exploration phase of its mission. By the end of 2013, Mars Hand Lens Imager (MAHLI) images revealed an unexpectedly high rate of damage to the rover wheels, which exceeded any damage observed during testing. Since then, the wheel wear and damage have been increasing. While the wheels were designed to operate with considerable damage, the rate at which damage was occurring was unexpected and raised concerns regarding wheel life expectancy [1]. With the knowledge gained from the MSL Curiosity Rover on wheel wear, as well as a better understanding of the terrain and the destructive surface on Mars, a new wheel design was necessary prior to the Mars 2020 (Perseverance) Rover launch.

During landing and traverse events, the rover wheels are the first structure to contact the Martian surface. As such, they are designed to act as a spring, or load mitigator, in order to minimize the loads that are transferred up to the rest of the rover body. The wheels are also the only structure available to minimize loads to the drive actuators. The wheels must be compliant enough to ensure that those delicate items survive, while still strong enough to not catastrophically fail during a landing event [2]. The MSL Curiosity and the Mars 2020 Perseverance Rovers, along with their predecessors, are equipped with six wheels and utilize a suspension known as rocker-bogie. The rocker-bogie suspension allows for the rover to drive over obstacles or through depressions that are as large as the wheels of the rover, with better tilt and stability.

Each wheel consists of an outer and inner rim, stiffening ring, wheel flexures (spokes) and skin grousers (treads), as shown in Figure 1. The wheel flexures provide a spring-like support for the wheel and drive actuators, while the skin grousers provide traction in the drive direction, as well as the traverse direction. The width of the wheel also plays an important role in preventing the wheel from sinking into the terrain. For both the MSL Curiosity and Mars 2020 Perseverance Rovers, each wheel was machined out of a block of flight-grade aluminum and equipped with titanium flexures. The Perseverance wheels are slightly larger in diameter than Curiosity's (20.7 in. vs 20.0 in.) and slightly narrower, with skin almost a millimeter thicker. The wheels also feature a new grouser design, which are slightly curved as opposed to a chevron-pattern, and there are twice as many (48 vs 24). Extensive testing in the Mars Yard at the NASA Jet Propulsions Laboratory (JPL) showed that the new treads better withstand the pressure from sharp rocks and grip just as well or better than Curiosity's when driving on sand and mitigate the fatigue failure mode of the Curiosity design [3].

Figure 1. MSL Curiosity and Mars 2020 Rover wheel design

Following the successful wheel redesign, there was a need to improve the characterization of and accurately model the overall wheel response, not only while traversing the surface of Mars, but more importantly during landing. As the rover touches down on the Martian surface, the wheels are subjected to large deformations and strains. An internal study was conducted at the JPL on the landing loads simulations, and it was observed that (1) uncertainty existed with how the wheel stiffness was accounted for and (2) the wheel stiffness was found to be a more significant contributor to landing loads than was initially expected. In response, the flexures were optimized to make them as soft as possible, while maintaining their structural integrity. Therefore, it became extremely important to properly characterize the stiffness and strength of the new wheel assembly to validate the landing loads simulation.

The redesigned Mars 2020 Rover wheel, along with the optimized flexures, was tested at the JPL using a mechanical ground support equipment (MGSE) cart with a hydraulic ram installed between the two, as shown in Figure 2. The setup was surrounded by a photogrammetry support frame onto which camera systems and lights were attached. The wheel static testing consisted of a total of 32 load cases. The first 30 cases pertained to the stiffness characterization, and the final two load cases served to qualify the wheel structure. Load cases in the stiffness characterization were selected to apply a wide array of loads at various locations around the wheel to broadly characterize the stiffness of the wheel assembly. The objective of the structural qualification was to achieve 1.2 x flight limit load (FLL) with no detrimental effects to the hardware and 1.4 x FLL without catastrophic failure of the test article. The wheel adapter plate was swapped out between load cases to clock the wheel and expose different clevis attachment points, while allowing the force/torque sensor to remain stationary. More detail surrounding the load application and nearby instrumentation can be observed in Figure 3.

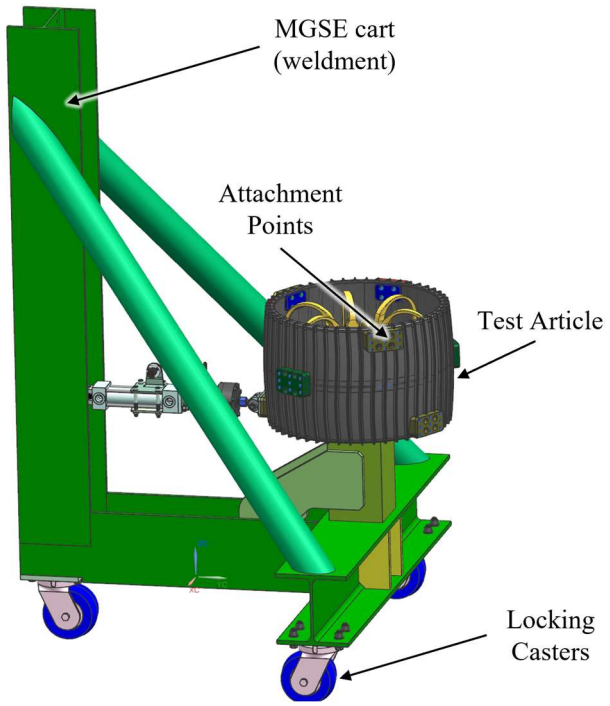

Figure 2. MGSE Cart with Hydraulic Ram and Test Article

A string potentiometer was used to monitor the overall load vs deflection behavior, while electrical-resistance strain gages and fiber optic strain sensors (FOSS) were utilized to monitor the overall strain behavior. Traditional instrumentation such as these, only allow for data to be collected at discrete locations, and therefore would not be sufficient on their own to provide all of the necessary validation data for the landing loads model. Therefore, full-field photogrammetry was required to complement the other instrumentation. Full-field photogrammetry has been successfully implemented on a few space vehicles in the past, including the composite crew module [4], an integrally stiffened composite aeroshell [5] and the Mars 2020 Heat Shield [6]. While studying the response of the integrally stiffened composite aeroshell, photogrammetry was able to clearly identify a manufacturing irregularity which could have been missed if traditional discrete-point instrumentation had been chosen instead of the full-field measurement.

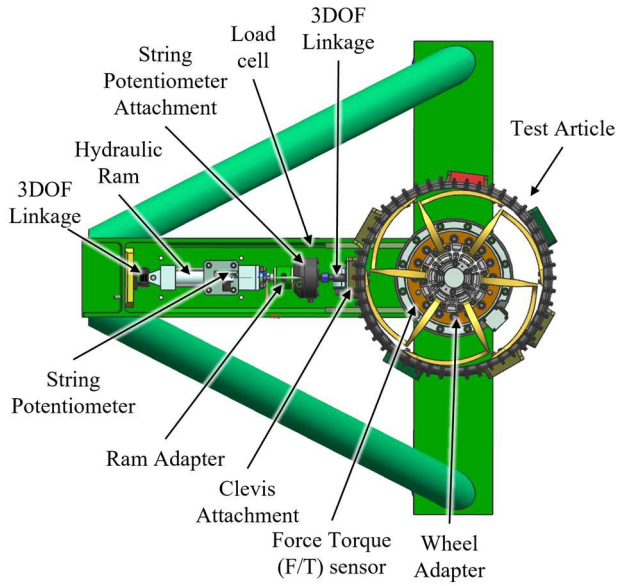

Figure 3. Load Application and Surrounding Instrumentation

The contents of this paper will focus on the implementation of three-dimensional, full-field photogrammetry, more specifically 3D-DIC, on the Mars 2020 Rover wheel assembly. Some of the challenges of this application and technique will be presented, along with how these challenges were overcome. The photogrammetry requirements, as well as the overall camera and test setup will be discussed in detail. Finally, examples of test-analysis correlation during the stiffness characterization and structural qualification will be presented.

2. Photogrammetry Requirements

Implementation of the photogrammetry technique to the Mars 2020 Rover wheel assembly testing was performed with two main objectives. The first objective was to monitor the wheel response in real-time, guarding against anomalous behavior and failure. In essence, this technique was used as a real-time non-destructive evaluation. The second objective was to provide test data for test-analysis correlation in order to validate and/or improve the high-fidelity computational model.

Some of the most important challenges that needed to be overcome for the successful implementation of full-field photogrammetry included:

(a) Extremely small available test area (footprint) at the JPL due to shared space with Dynamic Test Model (DTM) mobility deployment test setting up in the static-test tower area.

(b) Application of a speckle pattern to the complex geometry of the rover wheel assembly to provide the most accurate measurements.

(c) Merging of multiple camera views (systems) and their local coordinate systems into one global coordinate system that aligns with the finite element model (FEM).

3. Photogrammetry Implementation

In order to meet the first objective, critical areas of importance on the rover wheel assembly were selected by the JPL test team and stress analyst to be viewed and monitored in real-time using photogrammetry. To accomplish this, commercially available Digital Image Correlation (DIC) software, VIC-3D ™ [1], and four low-speed digital camera systems were positioned around the wheel assembly. One 29-MP (mega-pixel) system was positioned overhead viewing the wheel hub, flexures, and outer rim, while the other three systems (12-MP) were located circumferentially around the skin grousers (treads). Two of those systems were located at the load application point, while the third system was positioned 90 degrees from the load application point, to view the entire side of the wheel during loading and allow for sufficient overlap of the adjacent camera systems.

To satisfy the second objective, post-processed images from the four systems were merged (stitched) together under a common coordinate system. The coordinate system was then transformed to align with the FEM coordinate system. Full-field displacements and strains were then directly compared for test-analysis correlation.

The building block approach, as described in the following sections, was employed for optimizing measurement spatial resolution, overcoming the challenges mentioned above and ensuring seamless test operation.

3.1 Photogrammetry Camera Positioning

The first step in the building block approach involved building a photogrammetry test frame to mount the cameras, lights and cables, that would fit within the limited test area footprint at the JPL (see Fig. 4). In order to do so, an 80/20 aluminum extrusion frame was designed and constructed at NASA Langley Research Center (LaRC) to optimize the four photogrammetry camera systems with respect to each other and the desired field-of-view of the wheel assembly (for each system as shown in Fig. 5) to achieve full coverage and maximum resolution of the systems. The overall footprint of the 80/20 frame was approximately 8-feet long by 8-feet wide by 8-feet tall, with the main DIC support frame approximately 6-feet long by 6-feet wide by 8-feet. tall.

[1] *Specific vendor and manufacturer names are explicitly mentioned only to accurately describe the test hardware. The use of vendor and manufacturer names does not imply an endorsement by the U.S. Government, nor does it imply that the specified equipment is the best available*

A 3D printed to-scale model of the rover wheel assembly was sent to LaRC in order to verify the set-up and avoid delays during the actual test. More specifically, the 3D-printed wheel assembly was used to; (a) confirm the camera positions and layout, (b) verify the chosen speckle pattern for required field-of-view, depth of field and noise floor and (c) demonstrate merging/stitching of multiple camera views (systems) into one global coordinate system that aligns with the computational model.

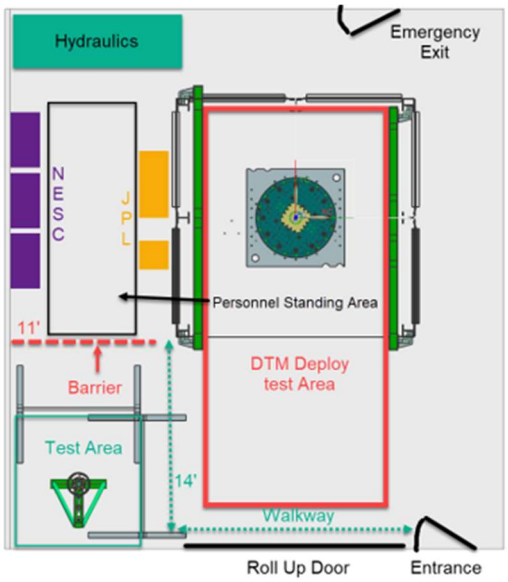

Figure 4. Limited Test Area Footprint at the JPL

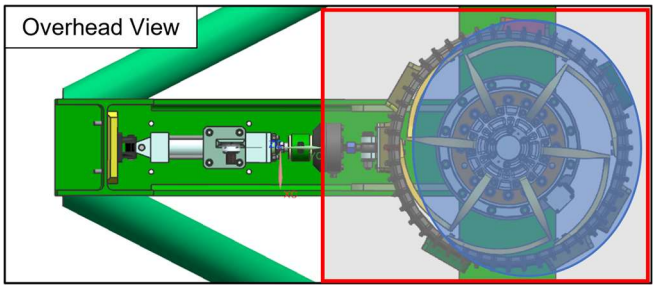

(a) 29-MP Overhead System

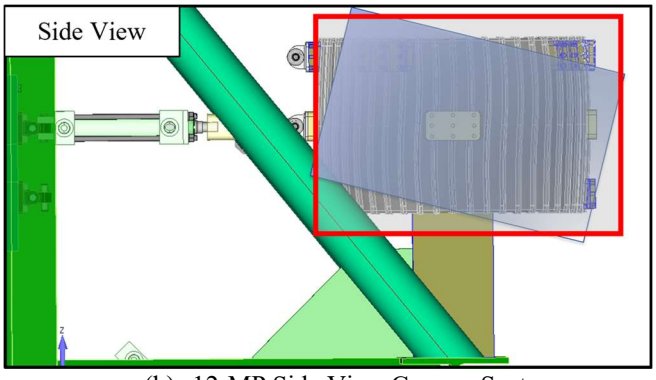

(b) 12-MP Side View Camera System

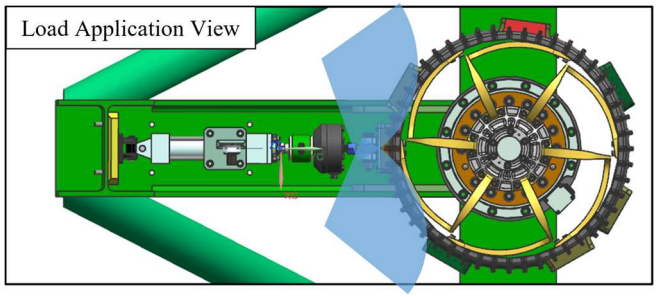

(c) 12-MP Load Application Camera System(s)

Figure 5. Desired Field-of-View for Each Photogrammetry Camera System

The photogrammetry test frame that was designed and fabricated at LaRC is shown in Figure 6. For this checkout, two camera systems were utilized to fulfill the mock-up requirements. An overhead 29-MP camera system was positioned above the 3D-printed wheel to view the wheel hub, flexures, and outer rim. Due to the symmetry of the 12-MP camera systems positioned around the circumference of the tire and skin grousers (treads), only one 12-MP camera system was necessary during checkout. The photogrammetry parameters that were calculated and successfully implemented are provided in Table 1.

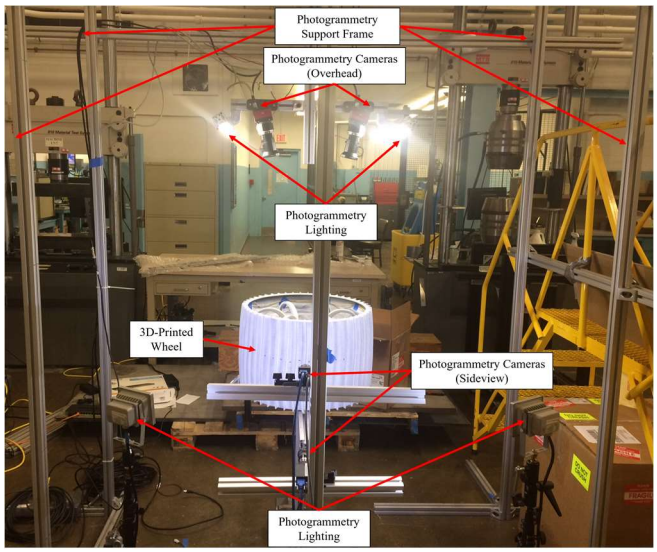

Figure 6. Photogrammetry Frame Designed at LaRC

Table 1. Calculated/Measured Photogrammetry Parameters

Camera Location	Field-of-View [in.]	Standoff Distance [in.]	Distance Between Cameras [in.]	Optimal Speckle Size [in.]
Overhead	36 x 24	30	14	0.025
Sideview	27 x 18	24	12	0.030
Load Application	18 x 12	16	8	0.020

3.2 Speckle Pattern and Validation

A typical structural DIC application requires a high-contrasting random speckle pattern (generally black speckles on flat white background) that is sprayed directly onto the surface of the test article to properly measures surface deformations and strains. The speckle size is a function of the camera resolution and field-of-view. Other parameters aside from the speckle pattern, such as lens type, aperture setting (depth-of-field), lighting, etc. [7] play an important role in surface measurement accuracy.

In order to apply the desired speckle pattern, a flat white spray paint was used to lightly cover the 3D-printed wheel assembly surface, while an airbrush was used to spray the desired speckle size(s). The airbrush was fit with a 0.016-in. (0.4-mm) needle and tip and used an acrylic black paint to generate the speckle size, with slight adjustments made to the needle to allow for a finer (smaller) speckle, or denser (larger) speckle depending on location on the wheel assembly. Due to the complex geometry of the rover wheel assembly, and difficulties of applying the optimal speckle pattern without structural interference, the wheel assembly was painted in parts and then re-assembled. A close up view of the 3D-printed wheel hub and spokes with an optimal speckle pattern applied can be observed in Figure 7.

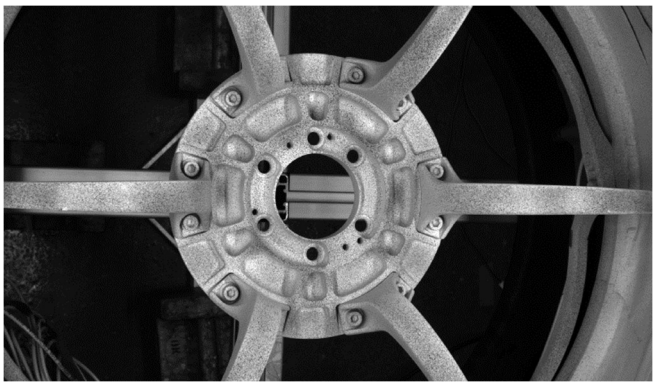

Figure 7. Close-up View of Speckle Pattern

To validate the applied speckle pattern (size, density, etc.) and measurement accuracy of the photogrammetry systems, as well as correlate the data with other instrumentation such as strain gages and FOSS, a tension test on a small titanium, Ti, coupon was performed (up to 7000 lbs.). Initially, photogrammetry was desired to view the inside of the wheel rim and the underside of the flexures, however due to the extreme complexity of this application, and the limited time frame, fiber optic strain sensors were utilized on those locations instead. A strain gage was also placed in the center of the Ti coupon, and the speckle pattern was applied over both the FOSS and the strain gage. Two 12-MP camera pairs, one viewing the front (strain gage-side) and the other viewing the back (FOSS-side), with 10 mm lenses, were positioned at similar distances as to what would be required for the side-view camera pairs at the JPL. The results generated between the DIC, FOSS and strain gage measurements are shown in Figure 8.

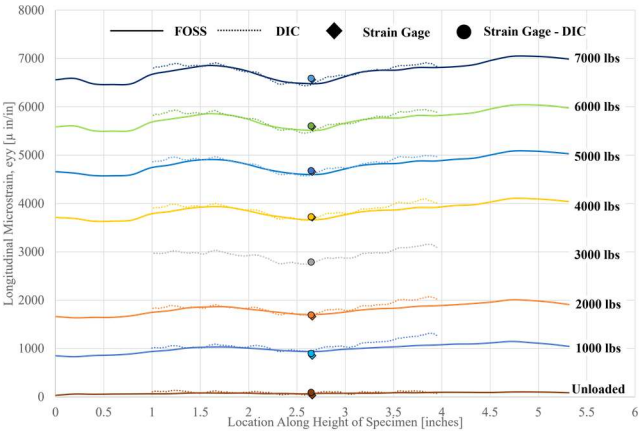

Figure 8. Comparison of the DIC, FOSS and Strain Gage Measurements

3.3 Multi-view Registration from Rigid Motion

Once the photogrammetry test frame was fabricated, along with proper camera layout, positioning, etc. and the optimal speckle pattern applied, the final step in the building block approach was to merge the data from the individual camera views (systems) into one global coordinate system that aligns with the computational model. In order to properly merge the data, a technique developed by Correlated Solutions, Inc., known as multi-view registration from rigid motion [8], was implemented. The principle behind using this technique is to calibrate multiple systems separately, use rigid motions of a speckle pattern to determine the geometric transformations between each system, and use this transformation to merge data into the same coordinate system.

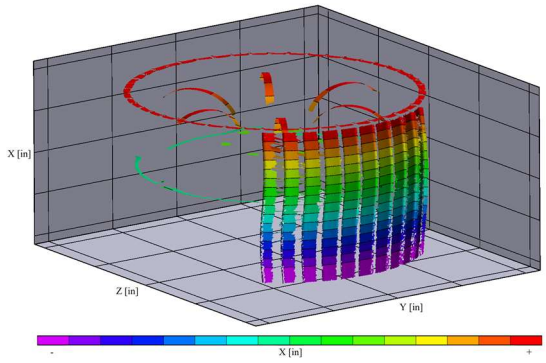

Figure 9. Merged Data-set Using MVR from RM

After both of the camera systems were properly calibrated, a rigid cylinder was used to generate the geometric transformations between the systems. 3M 1080-M10 vinyl vehicle wrap with a printed pattern, which was left over from the Mars 2020 Heat Shield acceptance testing [5], was applied to the surface of the cylinder and then the cylinder was translated and rotated while synchronized images were taken with the camera systems. To align with the FEM coordinate system, the overhead camera system was selected to be the primary system, i.e., the data from the other system(s) were transformed into the coordinate system of the overhead camera system. The merged (combined) data set

using the multi-view registration (MVR) from rigid motion (RM) technique is shown in Figure 9.

4. MARS 2020 ROVER WHEEL TEST SETUP

Once all of the photogrammetry-related parameters were established, verified and challenges overcome, the next phase of the work shifted towards the Mars 2020 rover wheel assembly testing at the JPL.

A complete material order list for the photogrammetry support frame, with exact dimensions of aluminum extrusion as measured and built at LaRC, along with mounting accessories and fasteners, i.e., gussets, pivot joints, cap screws and self-aligning nuts, was sent to the JPL to order and build prior to photogrammetry personnel arriving. In parallel to that effort, all of the other photogrammetry equipment, including lighting, cables, computers, function generator, fanout buffer/line driver, A/D board, calibration targets, etc. were shipped from LaRC to the JPL. The four camera pairs, along with camera mounts and lenses, were hand carried.

Two weeks prior to the start of testing, the complete rover wheel assembly (wheel hub, flexures and tire) was shipped from the JPL to LaRC to be instrumented with the FOSS, as well as painted and speckled for the photogrammetry. Each component of the wheel was individually packaged to make instrumenting the test article easier and essentially speed up on-site test set-up and assembly time. The FOSS was installed first, and then the wires/sensors were protected (masked) prior to the white base coat being applied. Masking was also carried out on other critical areas of the test article where assembly or friction contact was necessary to ensure no interference or surface contamination from the paint. Once the painting and speckle pattern was applied, and allowed to adequately dry, the individual parts of the Rover wheel were placed in a protective wrap and shipped back to the JPL for wheel assembly.

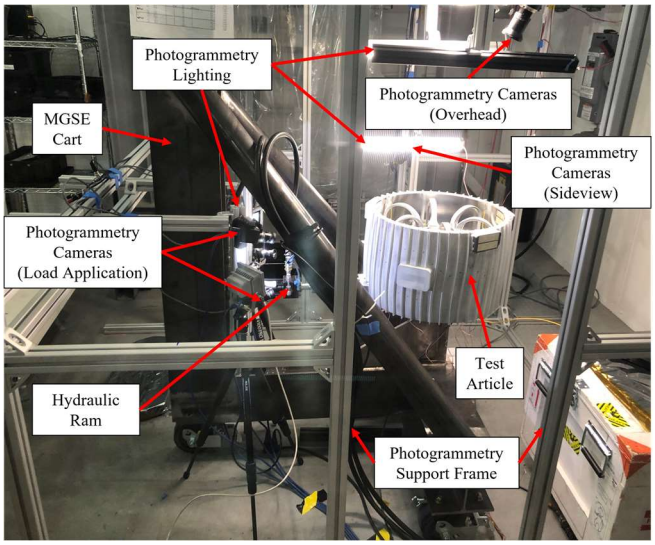

Figure 10. Photogrammetry Set-up at the JPL

Once on the JPL campus, cameras and lights were assembled and moved to their predetermined positions, as shown in Figure 10. Additional lighting was added to minimize shadows and improve the overall contrast of the test article. Two computers were required to run all four camera pairs, with the three 12-MP USB cameras recording data onto one computer, while the 29-MP GigE camera was recording onto the other. In order to properly sync all four camera systems, a 1 Hz square wave signal was sent from a function generator to the fanout buffer/line driver and then to trigger cables on the camera pairs. An A/D board was used to capture the load and displacement from the data acquisition system and this data was recorded with each DIC image captured. Images were acquired every second during loading and unloading, and approximately 30 images were acquired during the pre-determined load holds. This extended load hold was done for a few reasons; (1) allow for sufficient number of images to be recorded to reduce noise floor, (2) provide enough time to run FOSS scan, and (3) allow the test team to run spot checks of the photogrammetry displacement and strain measurement accuracy against traditional instrumentation and (4) give the stress analyst (test conductor) time to check their predictions against the full-field measured response.

4.1. Individual System Test Results

The static testing of the Mars 2020 Rover wheel assembly was conducted over the course of five days. The first four days involved the stiffness characterization which broadly characterized the wheel stiffness by varying load application points and incident angles and measuring the corresponding wheel behavior. The stiffness characterization was accomplished by applying load at three different rim locations (outer, middle and inner), at two clocking angles (on or between flexures) and five incident angles (+45, +22.5, 0, -22.5 and -45), resulting in 30 different stiffness load cases (Figure 11). It should be noted that for stiffness characterization, loads were selected such that all materials remain at least 20% below yield strain to protect the test article, even if analysis suggested there is ample capability to go beyond that load. The structural qualification testing was conducted on the fifth and final day of testing, where the wheel assembly was subjected to two critical load cases that were chosen by the JPL structures team, where the wheel assembly would be subjected to 1.2 x FLL and 1.4 x FLL, which would verify the ultimate capability of the wheel.

As mentioned earlier, one of the main objectives of the photogrammetry was to monitor the wheel response in real-time, guarding against anomalous behavior and failure. With a total of four camera systems and only two computers, only two systems could be chosen to run the real-time module of VIC-3D™. Based on discussion with the JPL test team and test conductor, the 29-MP overhead system was chosen, as well as one of the 12-MP systems viewing the load application point. The overhead system, viewing the wheel hub, flexures, and outer rim, was selected to monitor the large strain and displacements that were predicted analytically, while the camera system viewing the load application point

was selected to monitor the displacements of the tire and skin grousers (tread).

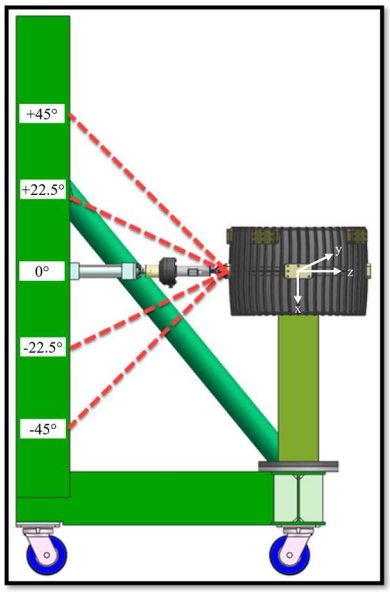

Figure 11. Load Application Points for Stiffness Characterization and Coordinate System

In order to meet the first main objective, pre-test predictions of the displacements and strains were produced at the maximum load level by the test team and a stress analyst at the JPL and these predictions/contour plots were available during testing. Also, pre-test line plots of displacement versus applied load were available for the entire time-history of the loading condition, to allow for spot checks during the ramp to maximum load. To enable real-time test-analysis comparisons, a common color scale was used for both the FEM predictions and the photogrammetry.

A typical test-analysis comparison of time-averaged (30 seconds worth of data during load holds) full-field x-direction displacement (defined as *U* in VIC-3D) at peak load is shown for one of the stiffness characterization cases, Load Case 6 (LC6), in Figures 12 and 13 for the overhead system, and Figures 14 and 15 for one of the systems viewing the load application point. This load case was selected due to the large amount of flexure displacement and tire rotation that was predicted/observed.

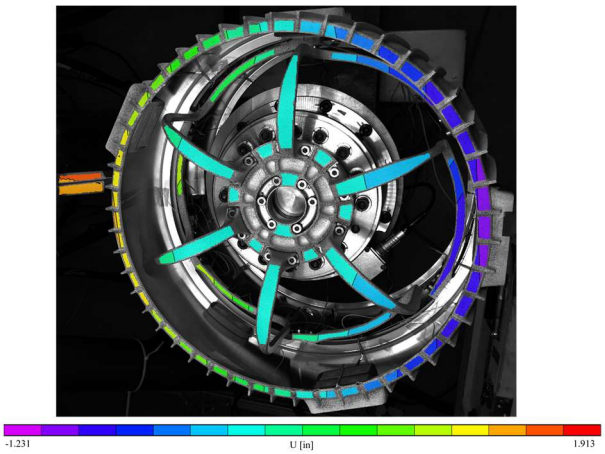

Figure 12. Peak Load X-displacement - Overhead (Test) – LS6

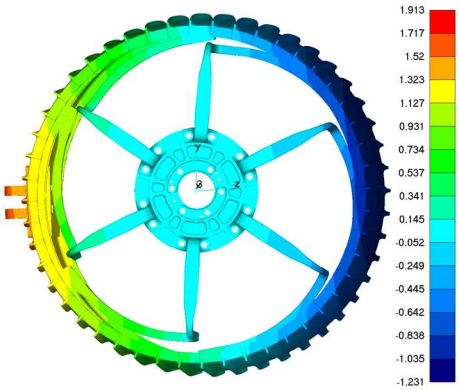

Figure 13. Peak Load X-displacement (Analysis) – LS6

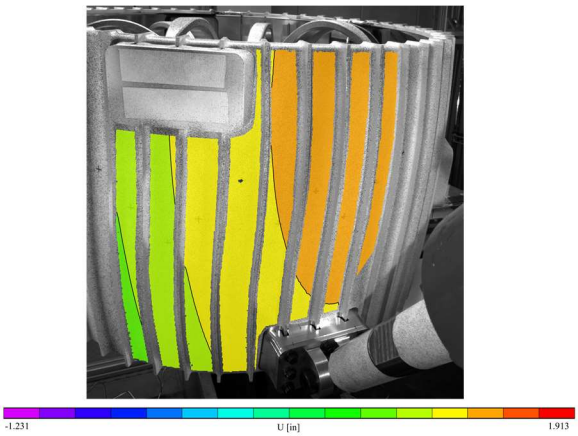

Figure 14. Peak Load X-displacement – Load Application Point (Test) – LS6

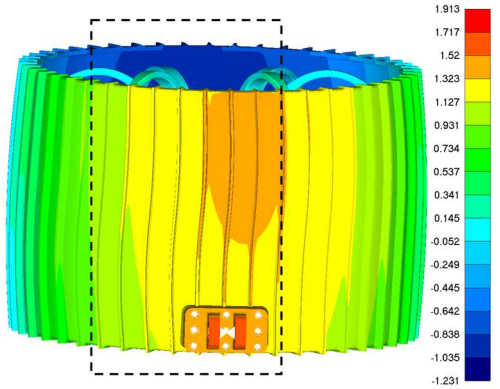

Figure 15. Peak Load X-displacement (Analysis) – LS6

While the real-time strain noise was of the order of ±150με, a much lower noise floor of post-processed (about ±50με) was achieved by time-averaging the data. Due to the complex geometry of the wheel and skin grousers, the strain data and contours were generated for the overhead system only. The test-analysis comparison of maximum principal strain, ϵ1, at the peak load for the qualification cases, LC31B and LC32B (1.4 x FLL) are shown in Figure 16 through Figure 20. These two load case were selected due to the large principal strain predicted/observed in the tire outer rim (LC31B) and flexures (LC32B).

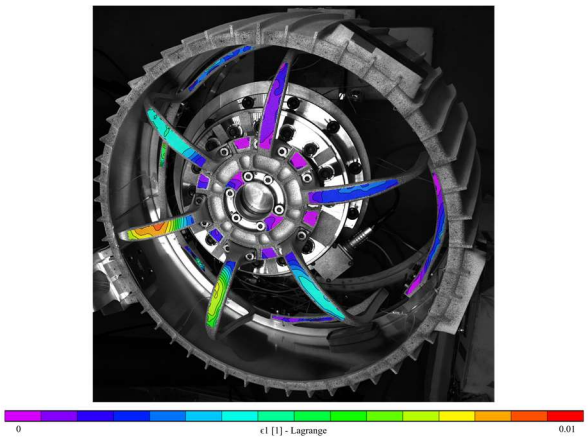

Figure 16. Peak Load Principal Strain, ϵ1 - Overhead (Test) – LS31B

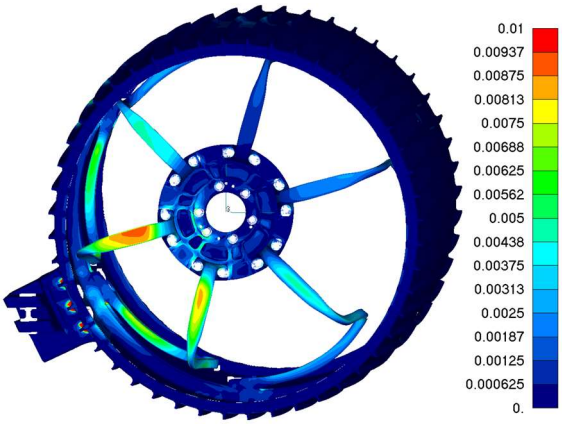

Figure 17. Peak Load Principal Strain, ϵ1 (Analysis) – LS31B

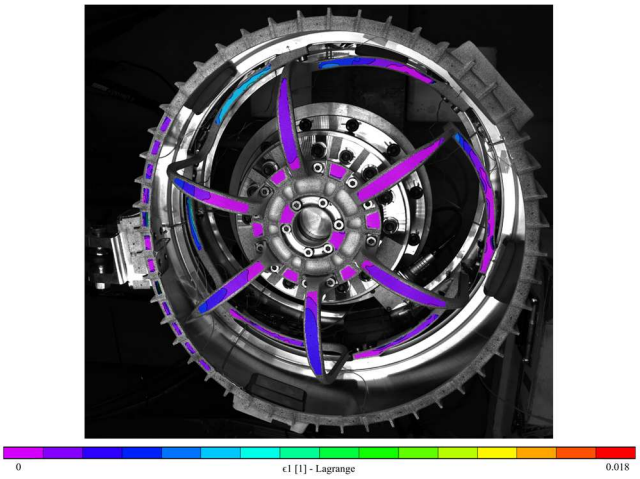

Figure 18. Peak Load Principal Strain, ϵ1 - Overhead (Test) – LS32B

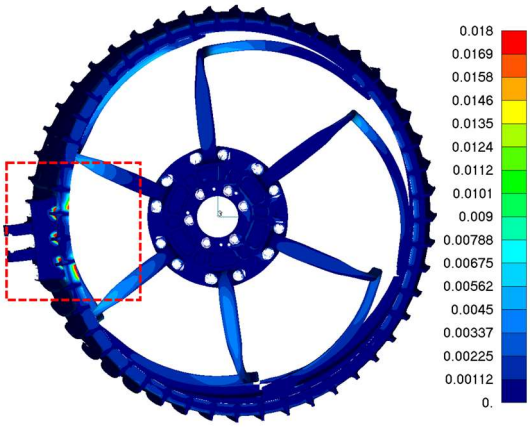

Figure 19. Peak Load Principal Strain, ϵ1 - (Analysis) – LS32B

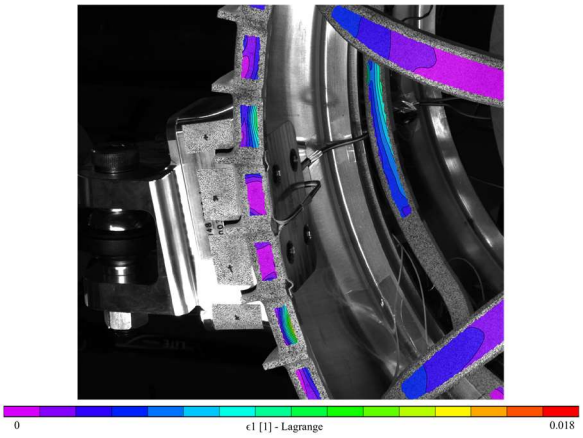

Figure 20. Peak Load Principal Strain, ϵ1 - Overhead (Test) – LS32B (Close-up View)

From these figures, it can be observed that the test and analysis are in excellent agreement. More specifically, the measured displacement and strain values, along with their respective contour gradients, are almost identical. The excellent correlation between test and analysis is even more

apparent in the maximum principal strain, $\epsilon 1$, values and gradients within the small width of the outer tire rim (0.375 in.), as shown in Figure 20.

4.2. Combined Test Results

The second main objective for the photogrammetry was to provide test data for test-analysis correlation to validate and/or improve the high-fidelity computational landing loads model. Following testing, individual photogrammetry system data was post-processed, merged into a global coordinate system, and presented in various formats to aid in the test-analysis correlation.

In order to meet this objective, a technique developed by Correlated Solutions, Inc., known as multi-view registration from rigid motion, was implemented. As mentioned earlier, this technique involves three steps; (1) Calibrate multiple camera systems separately, (2) Use rigid motions of a speckle pattern to determine the geometric transformations between each camera system, and (3) Use this transformation to merge individual system data into the same coordinate system. More specifically, the shape and deformation fields for each system were calculated separately and the geometric transformations were used to combine the data.

To improve on how this technique was used during the mock-up testing at LaRC, more specifically step (2) from above, a cylinder with a slightly larger diameter and height than the rover wheel assembly was 3D printed at the JPL. For the rigid motion of the speckle pattern, using a structure with almost identical dimensions as to those of the actual test article, allows for a more accurate merging of the data sets. The 3D printed cylinder with the vinyl speckle pattern applied is shown in Figure 21.

Figure 21. 3D-Printed Cylinder with Vinyl for Multi-view Registration (MVR) from Rigid Motion (RM) Technique

The overhead camera system was selected to be the primary system, i.e., the data from the other system(s) were transformed into the coordinate system of the overhead camera system, and then translated to align with the FEM coordinate system (origin at the center of wheel hub). The full-field x-, y- and z-direction displacements (*U*, *V*, *W* in VIC-3D) at the peak load for the 3D-merged data set (VIC-3D) versus the FEM prediction for one of qualification load cases, LC32B, are shown in Figure 22 through Figure 27 . It can be observed that there is excellent correlation between the full-field measured displacements of the merged photogrammetry data and the full-field predicted response.

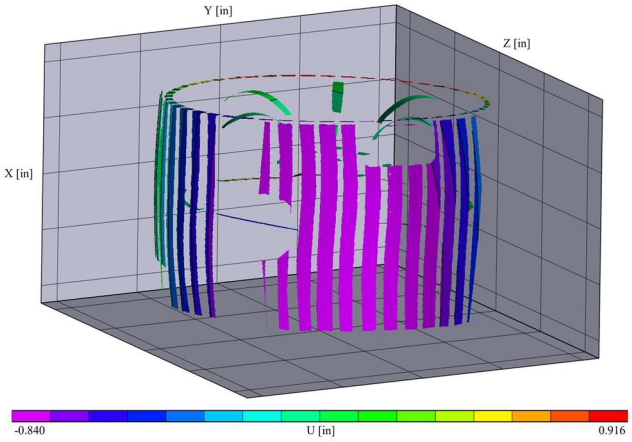

Figure 22. Peak Load X-displacement (Test) – LS32B – Merged Data Set

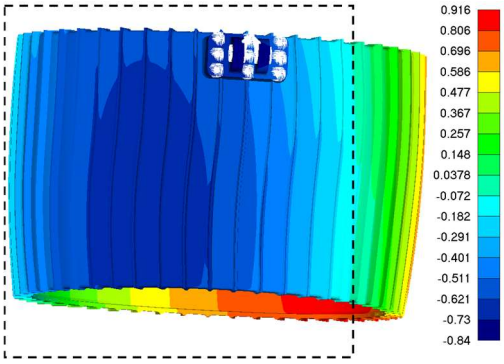

Figure 23. Peak Load X-displacement (Analysis) – LS32B

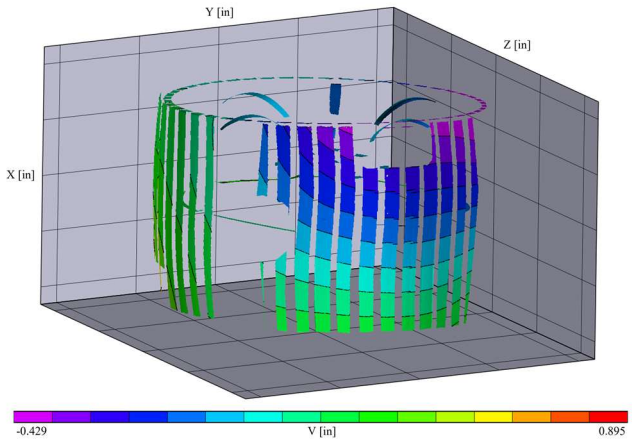

Figure 24. Peak Load Y-displacement (Test) – LS32B – Merged Data Set

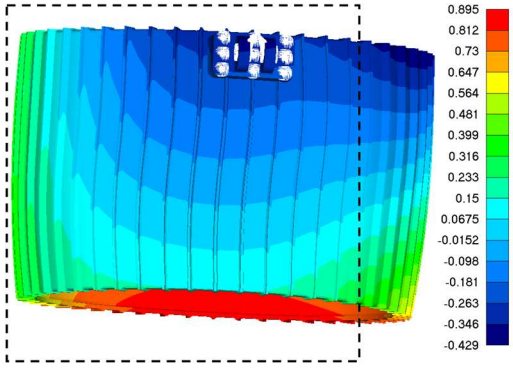

Figure 25. Peak Load Y-displacement (Analysis) – LS32B

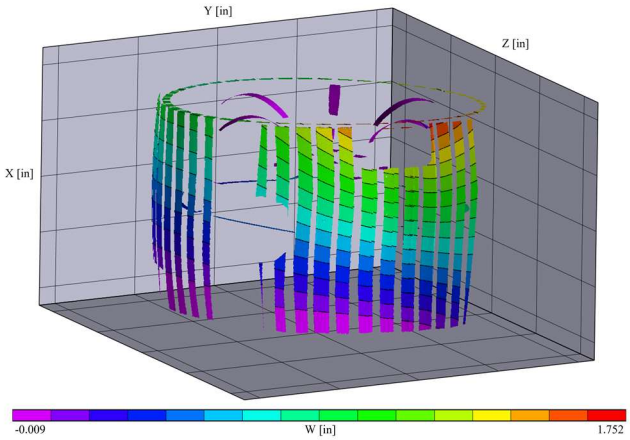

Figure 26. Peak Load Z-displacement (Test) – LS32B – Merged Data Set

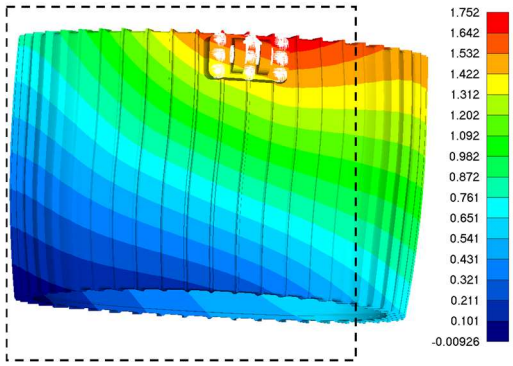

Figure 27. Peak Load Y-displacement (Analysis) – LS32B

As mentioned previously, due to the complex geometry of the tire and skin grousers, the photogrammetry strain measurements were extremely noisy, and therefore only displacement measurements would be made. With displacement as the primary measurement of digital image correlation, and strain being derived by differentiating the displacements, it can be assumed that agreement between the full-field displacements of the measured photogrammetry data versus the FEM predictions would correspond to an agreement between the full-field measured strains.

5. Summary and Discussion

5.1 Real-Time Monitoring and Significant Observations

With respect to the first main objective, the real-time monitoring of the displacements and strain worked as intended and the ability to monitor the response and guard against anomalous behavior at critical areas-of-interest was extremely useful. The photogrammetry proved invaluable for explaining otherwise anomalous strain gage readings, as well as other behavior not accounted for in the initial predictions, i.e., the manifestation of in-plane rotational slip mode of joints and flexure-to-flexure self-contact mode.

During one of the stiffness characterization load cases, a strain gage on one of the flexures was measuring much larger strains than the prediction (>750 με), and therefore an unplanned hold in loading was called. During this unplanned load hold, real-time strain measurements from the photogrammetry were compared with a FOSS scan and both showed strain measurements that were much closer to prediction (<150 με). After confirming this erroneous reading from the strain gage, it was determined that the strain gage may not be in direct contact with the surface, and therefore the strain reading was disregarded, and the load case was continued and completed.

Several load cases presented rotation of the flexure foot in the plane of the flexure foot,/tire interface. After observing this phenomenon in the first stiffness characterization load case, it was found that this rotational slip could be predicted to approximately 10% of the load when it was observed. This effect was very visible across multiple data sets and can be alarming if it is not anticipated. Upon unloading of the wheel assembly, the photogrammetry was able to measure residual deformation and strains, which agreed with the string potentiometer, strain gage and FOSS measurements.

There is a flexure-to-flexure self-contact mode that can manifest when the wheel is loaded in certain orientations, and this was not always anticipated in the initial test predictions. It was identified prior to the final structural qualification test, LC32, that due to the specific loading conditions, flexure-to-flexure self-contact would occur. Though predictions could be adjusted to account for this contact, there were no strain gages in the impacted vicinity to gage if local behavior was consistent with those predictions or not. Fortunately, this area was in the observable field of the photogrammetry system and was monitored closely in real-time, capturing the flexure-to-flexure self-contact and testing proceeded nominally.

Had it not been for the full-field photogrammetry, and real-time monitoring of the wheel assembly, effectively monitoring against anomalous behaviors such as these, strain gages would have needed to be replaced and cameras re-positioned to view the areas of flexure-to-flexure self-contact. In the absence of the photogrammetry, the testing would have been stopped for a few days to install additional strain gages, and to reconfigure and recalibrate the

photogrammetry systems. Having the real-time photogrammetry available allowed for anomalous behavior and potential failure modes to be monitored, verified with other instrumentation as real or erroneous, and testing to continue without any delay in schedule.

5.2 Merged Data Set for Test-Analysis Correlation

With respect to the second main objective, having the ability to combine the data sets from multiple camera systems into one global coordinate system to align with the FEM offered a unique opportunity to view the entire wheel assembly response at a given load hold and compare directly with the model predictions. Excellent test-analysis correlation for a given camera system can be observed in Figure 12 through Figure 20, however, to fully validate the model, it is important to see the entire wheel behavior and ensure all of the measured data from the individual photogrammetry systems agree with the analysis. The test-analysis correlation of the full-field displacements, as shown in Figure 22 through Figure 27, are in excellent agreement, which along with the other instrumentation helps to validate the high-fidelity computational landing loads model.

6. CONCLUSIONS

3D full-field photogrammetry was successfully implemented during the static loading of the Mars 2020 rover wheel assembly. The challenges that were addressed during set-up, testing and post-processing were all overcome to provide the most accurate photogrammetry data. Full-field deformations and strains were monitored in real-time using four low-speed photogrammetry systems and acted as a form of real-time non-destructive evaluation. Post-test time-averaged data from these individual systems were merged into a single coordinate system to align with the FEM improved test-analysis correlation and to better observe any discontinuities between the measured response and the predicted response. Overall, there was excellent agreement between the test-analysis for the stiffness characterization and structural qualification testing and all objectives of the static test were met successfully.

REFERENCES

[1] E. Graser, S. McGill, A. Bielawlec and A. Rankin, "Rimmed Wheel Performance on the Mars Science Laboratory Scarecrow," IEEE Paper 2019, IEEE Aerospace Conference, Big Sky, Montana, March 2019.

[2] S. Haggart and J. Waydo, "The Mobility System Wheel Design for NASA's Mars Science Laboratory Mission," 11th European Conference of the International Society for Terrain-Vehicle Systems, Torino, Italy, November 2008.

[3] S. J. Mraz, "NASA's Latest Martian Rover Gets New Wheel and a Brake Job," Machine Design, April 8, 2020. https://www.machinedesign.com/markets/robotics/article/21128286/nasas-latest-martian-rover-gets-new-wheels-and-a-brake-job. Accessed September 2022.

[4] M. T. Kirsch, "Composite Crew Module: Test," NASA/TM-2011-217190, NESC-RP-06-019.

[5] S. Kellas, "Integrated Composite Stiffener Structure (ICoSS) Concept for Planetary Entry Vehicles," 57th AIAA/ASCE/AHS/ASC Structures, Structural Dynamics and Materials Conference, San Diego, California, January 2016.

[6] S. Kellas, D. S. Dawicke, N. W. Gardner, M. P. McNeill, W. M. Johnston, B. A. Jabola, D. M. Shannon and M. M. Abid, "Real-Time Full-Field Photogrammetry Implementation During the Mars 2020 Heat Shield Acceptance Test," IEEE Paper 2020, IEEE Aerospace Conference, Big Sky, Montana, March 2020.

[7] A Good Practices Guide for Digital Image Correlation, International Digital Image Correlation Society, October 2018.

[8] Correlated Solutions, Inc., "Application Note: AN-1804 – Multi-View Registration from Rigid Motions," https://correlated.kayako.com/article/73-multi-view-registration-from-rigid-motions. Accessed October 2022.

ACKNOWLEDGEMENTS

The authors wish to acknowledge Chris Landry and Peyman Mohasseb, Mars 2020 structures lead and structures group supervisor, respectively, for being the NASA JPL internal advocates for understanding the importance of the 3D-DIC technique and requesting it to be utilized on the wheel static test. The authors also wish to acknowledge Patrick DeGrosse, Mars 2020 mobility system cognizant engineer for supporting the additional complexity and logistics required to employ the photogrammetry.

BIOGRAPHY

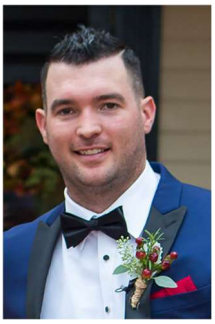

Nathaniel W. Gardner *is a Research Aerospace Engineer working within the Structural Dynamics Branch, more specifically the Landing and Impact Research (LandIR) Facility, at NASA Langley Research Center (LaRC). With over 15 years of Digital Image Correlation and R&D experience, he specializes in structural dynamics and aircraft crashworthiness, with an emphasis on utilizing photogrammetry, along with traditional instrumentation, to better understand and characterize the structural response. Dr. Gardner received both his undergraduate degree (B.S.M.E.) and Ph.D. (M.E. - Solid Mechanics) from the University of Rhode Island in 2007 and 2012, respectively. Since joining NASA in 2013, Dr. Gardner has worked on numerous projects, including the testing and analysis of the Mars 2020 Heat Shield, Mars 2020 Rover wheel, Orion Heat Shield, Space Launch System (SLS),*

Frangible Joint Empirical Testing (FJET), Shell Buckling Knockdown Factors (SBKF) and Multi-Bay Box (MBB) for a Blended Wing design.

***Jon Hamel** is a structural engineer in the Spacecraft Structures and Dynamics group at the NASA Jet Propulsion Laboratory (JPL). He joined JPL in 2016 to support the design, analysis and structural testing of the Perseverance Rover for the Mars 2020 program and is currently supporting the structural analysis and testing for the Europa Clipper program. He began his career in 2007 at the Boeing Satellite Development Center in El Segundo, California supporting the production, structural analysis, and anomaly investigations of a variety of spacecraft structures, antenna feeds, reflectors, and microwave hardware. He received a B.S., in Aerospace Engineering and a M.S. in Structural Mechanics from the University of California, Los Angeles.*

***Sotiris Kellas** received a B.S., in Aeronautical Engineering, an M.S. in Structural Mechanics and a Ph.D. in Composite Material and Structures from Imperial College, London England. He has been with NASA Langley Research Center (LaRC) for over 15 years. He began his career in 1988 as Visiting Assistant Professor at Virginia Tech before joining Lockheed Martin and then General Dynamics to provide research support for NASA. In addition to participating in many NASA Engineering and Safety Center (NESC) investigations, he was the test lead for the Composite Crew Module, Composites for Exploration, and the Alternate Heatshield Carrier Structure design for the Orion crew module. Dr. Kellas has published dozens of technical papers and NASA reports in the area of composite structures design, fabrication and testing. Currently, he is the structures lead for several Earth Entry Vehicle projects.*